JOURNAL OF MATERIASLS SCIENCE 33 (1998) 2583–2588

# Influence of TiC additions on the oxidation behaviour of $Si_3N_4$-based ceramics

A. OPSOMMER, E. GOMEZ*, F. CASTRO
*Centro de Estudios e Investigaciones Técnicas de Guipuzcoa, P Manuel de Lardizabal 15, 20009 Donostia, Spain*
**Escuela Universitaria Ingenieria Tecnica Minera (Euskal Herriko Unibertsitntoa, Fisika Saila), Colina de Beurko s/n, Barakaldo (Bizkaia), Spain*
*E-mail: Fcastro@ceit.es*

The oxidation behaviour in air of $Si_3N_4$ ceramics containing $Y_2O_3$ and $Al_2O_3$ as sintering aids, with and without a dispersion of TiC particles, has been studied between 1200 and 1400 °C. The influence of TiC additions on the oxidation kinetics is discussed in comparison with the results obtained for the $Si_3N_4$–$Y_2O_3$–$Al_2O_3$ reference material. However, in all cases and within the experimental temperature range, the oxidation kinetics were observed to be of a parabolic type. The microstructure of the oxide scales formed, which has been characterized by scanning and transmission electron microscopy, was observed to depend on the oxidation temperature and the initial composition of the material.


## 1. Introduction

It is well known that the oxidation of non-oxide ceramics has a great influence on their high-temperature properties and may limit their use in structural applications [1, 2]. Composite materials based on $Si_3N_4$ with additions of TiC, TiN or HfC particles have been developed for use as tools in machining operations and wear resistant components in order to reduce the problems of chemical wear and abrasion [3, 4]. While the oxidation behaviour of either hot isostatically pressed or sintered $Si_3N_4$ with additions of MgO, other metallic oxides or rare-earth elements has been extensively studied [5–7], relatively little has been reported on the influence of Ti carbides and nitrides on the oxidation process [8, 9]. Those studies describe some characteristics of the oxidation behaviour of $Si_3N_4$–TiN composites. However, the present work presents a detailed characterization of the microstructural characteristics of the oxide products formed and its relation with the overall oxidation kinetics of $Si_3N_4$ based ceramics with TiC additions.

## 2. Experimental procedure

Sintered $Si_3N_4$ with additions of $Y_2O_3$ (6 wt%) and $Al_2O_3$ (1.5 wt%) was used as a baseline material. Composites were formed by adding particles of TiC. Powder mixtures produced by ball milling (48 h) were uniaxially pressed at pressures of 50 MPa to obtain samples with a green density between 54 and 65% of the theoretical density. Samples of 96–97% of the theoretical density were obtained by sintering at 1900 °C under $N_2$ at 5 bar for 60 min in a furnace with a graphite heating element. A powdered bed consisting of equal proportions of $Si_3N_4$ and BN was used in all cases during sintering in order to prevent the thermal decomposition of the experimental materials. After polishing the samples to a final finish of 1 μm, they were oxidized in air at atmospheric pressure at temperatures between 1200 and 1400 °C. After oxidation, mass gains per unit area were determined and the structural characteristics of the oxide scales examined by X-ray diffraction (XRD), scanning electron microscopy (SEM) and transmission electron microscopy (TEM). All the electron diffraction patterns were obtained using an accelerating voltage of 100 kV.

## 3. Results

### 3.1. Microstructure of the as-sintered materials

The microstructure of the experimental materials with a chemical composition of $Si_3N_4$–6 wt% $Y_2O_3$–1.5 wt% $Al_2O_3$ consists of prismatic grains of β-$Si_3N_4$ (equivalent diameter of 1.7 μm and aspect ratio of about 5.5) and an (Y–Al–Si)-containing intergranular phase which mostly crystallized as α-$Y_2Si_2O_7$ with small amounts of apatite. Based on XRD data the composition of the β-$Si_3N_4$ was determined to be $Si_{5.92}Al_{0.08}O_{0.08}N_{7.92}$, which corresponds to a sialon type of the β′-$Si_3N_4$ structure.

The composites with TiC exhibited a finer microstructure consisting of β′-$Si_3N_4$ grains with a mean size of 1.4 μm and an aspect ratio of about 6, $TiC_{0.6}N_{0.4}$ grains with a mean size of 1.2 μm and a ($4Y_2O_3$–$SiO_2$–$Si_3N_4$) (N–YAM) intergranular phase.

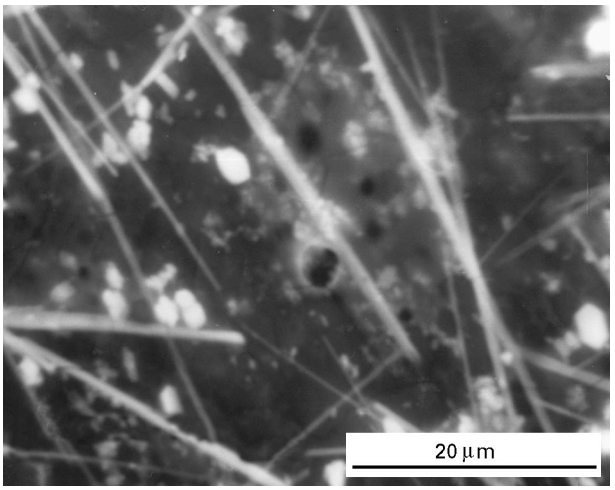


*Figure 1* SEM image from the surface of the oxide scale after oxidation at 1200 °C.

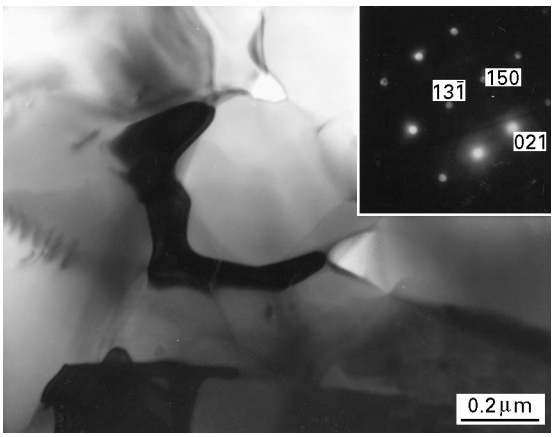


*Figure 2* TEM micrograph and electron diffraction pattern (inset) ($L = 405$ mm) of $\gamma$-$Y_2Si_2O_7$ precipitates formed at the interface between the sublayers which constitute the oxide scale.

## 3.2. Structure of the oxide-scales

In the two types of material, several differences in the oxide scales were identified depending on the chemical composition of the materials. As can be seen in Fig. 1, on samples without TiC the surface of the oxide product consisted of cristobalite, Y disilicates, apatite and porosity, which is believed to have been formed during the oxidation of quaternary phases. As reported before [10], at high oxidation temperatures the oxide scales are formed with a layered structure. Basically two main layers were distinguished: the outer layer containing highly textured crystals of $Y_2Si_2O_7$ and cristobalite embedded in a glassy phase (Fig. 1) and an inner layer next to the substrate where $Si_3N_4$ and $Si_2N_2O$ coexist. The interface between these layers (Fig. 2) is characterized by the formation of $Y_2Si_2O_7$ crystals of irregular form and the presence of bubbles which presumably form owing to the release of $N_2$ or NO from supersaturated glass. From XRD analysis it was noted that after an initial period, which corresponds to the formation of $Si_2N_2O$ as a primary oxidation product, the ratio of the intensities of the 2 0 0 and 1 1 1 reflections

TABLE I Change in the $I_{1\,1\,1}(Si_2N_2O)/I_{2\,0\,0}(Si_3N_4)$ ratio with time at 1250 °C

| Time (hours) | $I_{1\,1\,1}(Si_2N_2O)/I_{2\,0\,0}(Si_3N_4)$ |
|---|---|
| 0 | 0.015 |
| 1.5 | 0.03 |
| 2.5 | 0.042 |
| 17 | 0.038 |
| 25 | 0.046 |
| 48 | 0.042 |

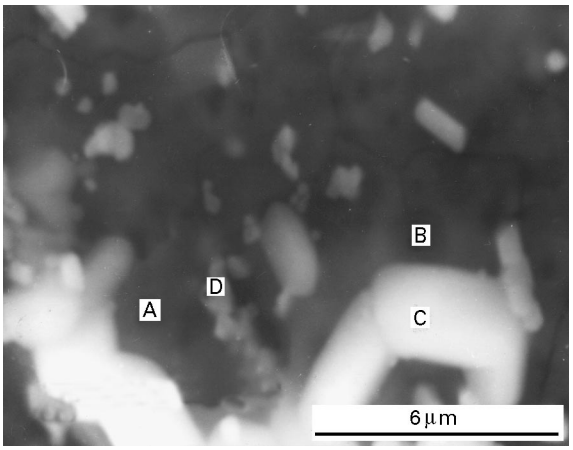


*Figure 3* STEM image of the outer layer of the oxidation scale formed in materials with 10%TiC additions. A, crystals of $SiO_2$; B, glassy phase; C, crystals of $TiO_2$; D, $Ti_2Si_2O_7$.

of $Si_3N_4$ and $Si_2N_2O$, respectively, remains constant, indicating that the thickness of the inner layer does not significatively change with the oxidation time (Table I).

For the material containing additions of TiC particles a layered structure of the oxide scale was also observed after high-temperature oxidation. It is also noteworthy that the oxidation of TiC, to form $TiO_2$, was observed to take place at temperatures between 450 and 1100 °C. In this case the oxide scale consisted of three sublayers. The outermost layer formed by $SiO_2$, as cristobalite and keatite, $TiO_2$ in tetragonal and orthorhombic form and small crystals of $Ti_2Y_2O_7$ which are formed as a result of the reaction between $TiO_2$ and $Y_2O_3$. All these phases were observed to be embedded in a glassy phase. An example of this layer is shown in the scanning transmission electron microscopy (STEM) image in Fig. 3. TEM images and the corresponding diffraction patterns of some of these phases are shown in Fig. 4. The experimental observation that the concentration of Ti in the two outer layers is much higher than next to the substrate indicates that ions of $Ti^{3+}$, as do those of additive and impurity elements, diffuse outwards during the oxidation process (Table II). In the mid-sublayer, Ti was found to be present as $Ti_2Y_2O_7$, unreacted TiC crystals and Ti oxides with a valence less than 4. The coexistence of these phases may be understood on thermodynamics grounds, as illustrated in Fig. 5 which shows the fields stability of Si–O–N phases as a function of $P_{N_2}$ and $P_{O_2}$ together with the pressures

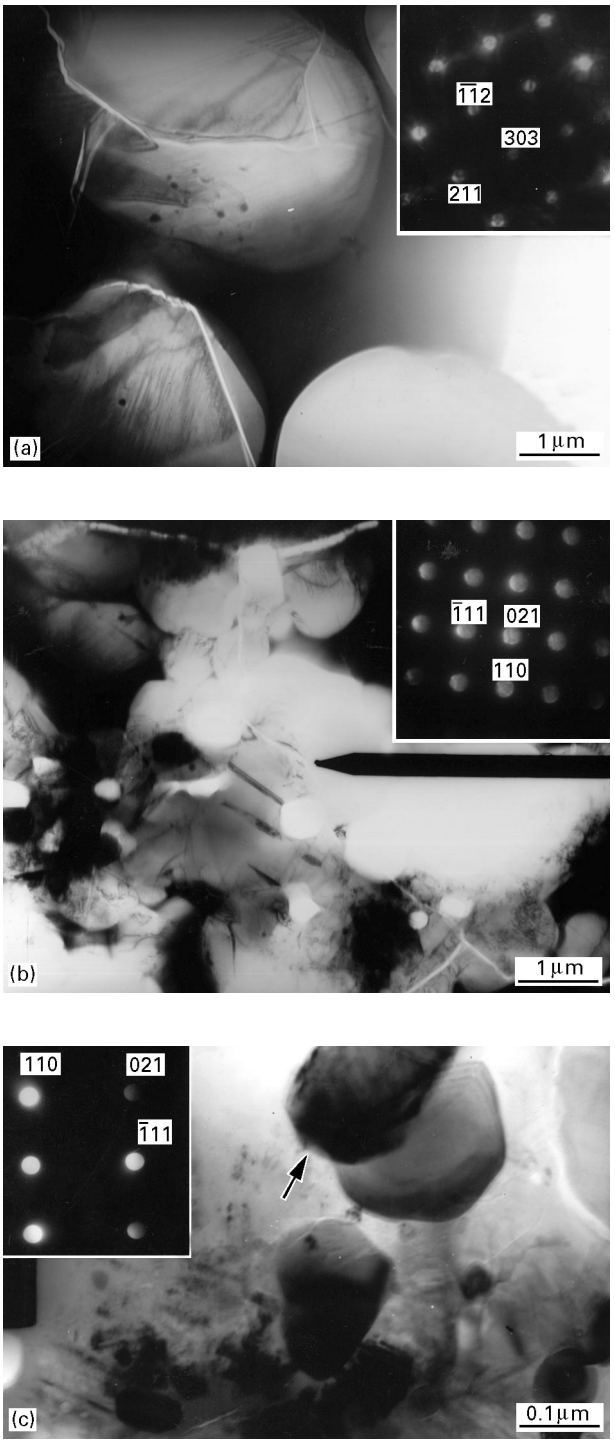


*Figure 4* TEM images and electron diffraction patterns (insets) corresponding to crystals of (a) cristobalite ($L = 555$ mm), (b) keatite ($L = 795$ mm) and (c) rutile ($L = 795$ mm) contained on the surface of the oxide scale.

corresponding to the conversion of TiC in $Ti_2O_3$ and $Ti_2O_3$ in rutile for two different $P_{CO_2}$ values. Fig. 6 shows the identification of these phases by electron diffraction. The sublayer next to the substrate had a marked resemblance to the corresponding layer in the material without TiC additions.

### 3.3. Kinetics

In the experimental range of oxidation temperatures the kinetics are parabolic as shown by the typical plot

TABLE II Chemical composition of the oxide layers on a composite with TiC: composition of the material before oxidation, $Si_3N_4$–6 wt% $Y_2O_3$–1.5 wt% $Al_2O_3$–2 wt% TiC; oxidation conditions, 1200 °C, 72 h

| Element | Element concentration in the oxide layers (wt%) | | before oxidation (wt%) |
|---|---|---|---|
| | Outer sublayer | Inner sublayer | |
| Al | 1.2 ± 0.2 | 0.1 ± 0.2 | 1.3 |
| Si | 51.4 ± 0.5 | 72.6 ± 1.9 | 83.1 |
| Y | 9.1 ± 0.2 | 18.5 ± 1.8 | 2 |
| Ti | 38.4 ± 0.6 | 7.8 ± 0.6 | 13.5 |

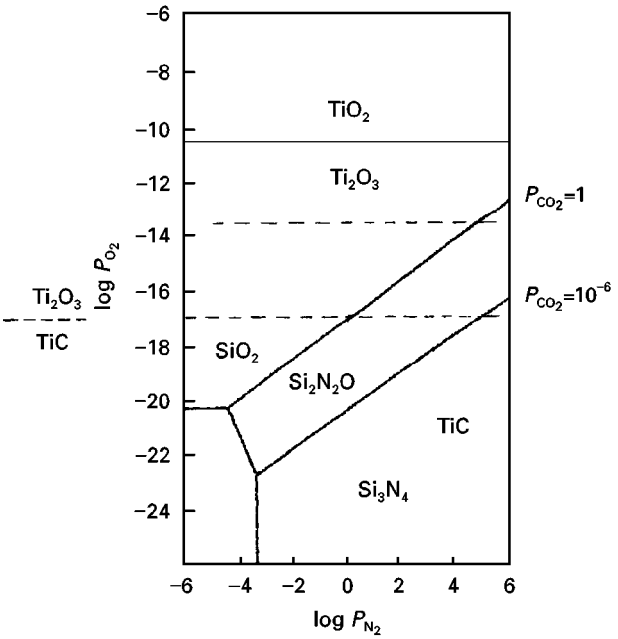


*Figure 5* Stability diagram of Si compounds and conditions for the conversion of TiC and $Ti_2O_3$ into $TiO_2$.

of the mass gain per unit area versus time shown in Fig. 7. The figure shows a rapid initial mass gain followed by a much lower secondary stage. Fig. 8 summarizes the experimental data obtained up to an oxidation temperature of 1400 °C. This data was used to obtain the temperature dependence of the reaction constants, which is shown in Fig. 9. From this plot an apparent activation energy of 460 kJ mol$^{-1}$ for the reference material ($Si_3N_4$–6 wt $Y_2O_3$–1.5 wt% $Al_2O_3$) was obtained. This value adequately compares with previously reported data based upon metallic cation migration as the controlling mechanism for the oxidation process. [11, 12].

As seen in Fig. 10, in spite of the addition of TiC the apparent activation energy for the oxidation process in the composite material does not significantly change and the measured values (450–460 kJ mol$^{-1}$) are comparable with those reported by others for composites containing TiN additions [9].

## 4. Discussion

As demonstrated by the TEM work carried out on thin foils of the oxide scales formed in the two experimental

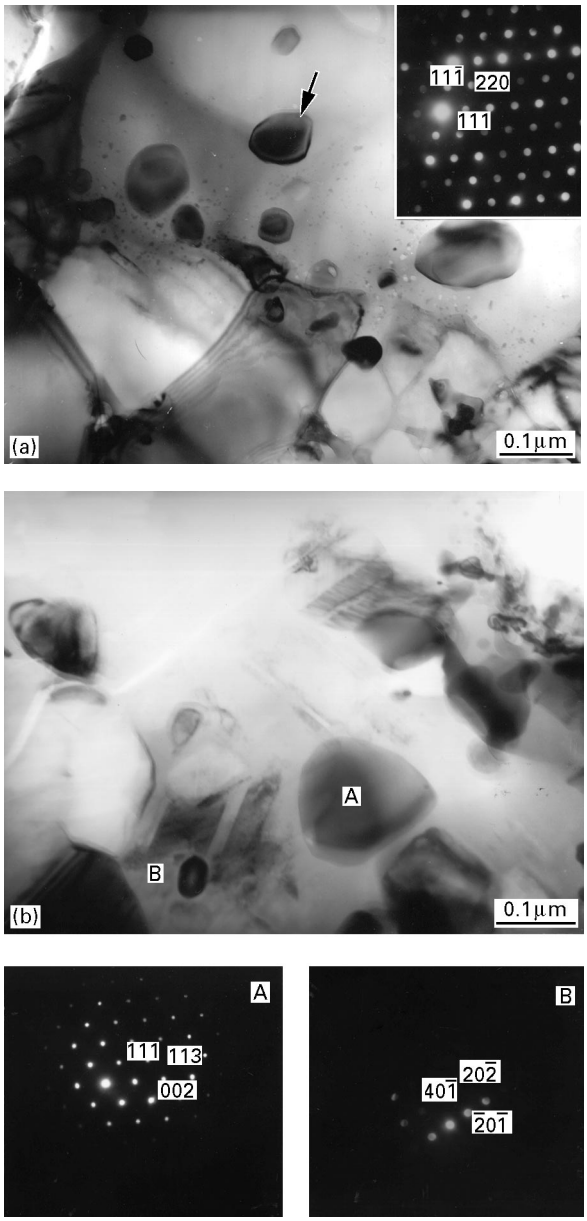


*Figure 6* TEM images and electron diffraction patterns ($L = 555$ mm) of phases present in the inner layer of the oxide scale: (a) TEM image of $Ti_2Y_2O_7$ with corresponding electron diffraction patern (inset) and (b) TiC, (labelled A) and $TiO_2$ (labelled B) with correponding electron diffraction patterns of A and B.

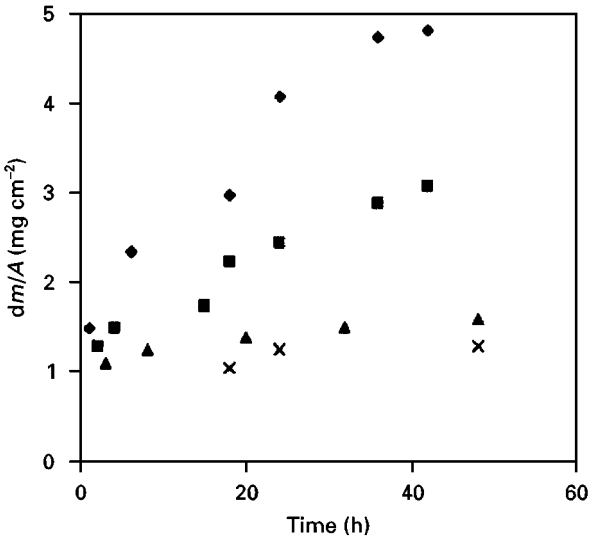


*Figure 7* Mass gain per unit area versus time for all the oxidation temperatures used in this work for the base material. (◆), 1400 °C; (■), 1350 °C; (▲), 1300 °C; (×), 1250 °C.

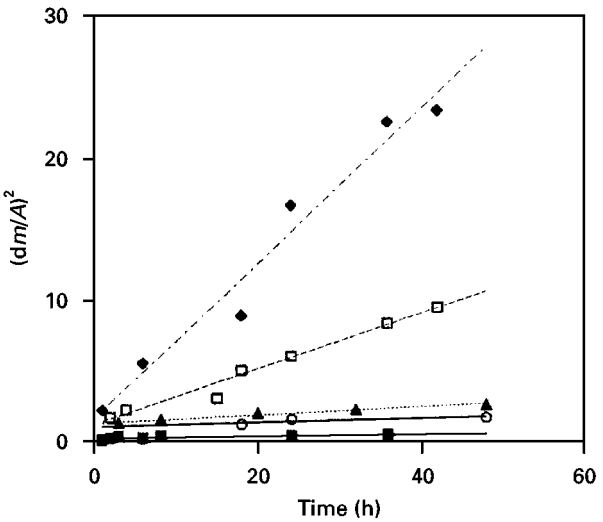


*Figure 8* Parabolic relationship between mass gain and time during oxidation of the base material. (◆), 1400 °C; (□), 1350 °C; (▲), 1300 °C; (○), 1250 °C; (■), 1200 °C.

materials, it is clear that such oxide scales change, in both chemical composition and microstructure from the reaction interface, in contact with the substrate, to their surface in contact with air. From these analyses it is apparent that at least two sublayers, formed within the oxide scale, are the constituents of the oxide scale as a whole. The basic difference between the oxide scales formed in each material obviously depends on the original chemical compositions of their substrates. It must be emphasized, however, that the introduction of TiC into the reference material does not seem to have a strong effect on the overall kinetics of oxidation, which are essentially governed by the formation of a passivating oxide layer, thus resulting in a parabolic type of kinetics in all the experimental temperature range. Nonetheless, at the same oxidation temperature, samples containing TiC exhibited larger mass gains as can be appreciated by the plot in Fig. 11. It is also noteworthy that, according to the results shown in Fig. 10, the activation energy for the oxidation process is essentially the same to a good degree of approximation for all the experimental materials, despite their TiC content.

The observations of the internal formation of a layer with $Si_3N_4$ and $Si_2N_2O$ in the reference material can be explained on the basis of the model proposed by Clarke [13] for internal oxidation, as presented schematically in Fig. 12.

The outer cover forms by the conversion of $Si_3N_4$ and $Si_2N_2O$ into $SiO_2$ and its rate of formation depends on the diffusion of oxygen through the forming layer of $SiO_2$. Neglecting the changes in thickness due to the crystallization of Y compounds, the growth rate of this layer will be given by

$$\frac{dx}{dt} \approx \frac{D_{O_2}(P_{O_2(atm)} - P_{O_2(l_2)})}{dx}$$

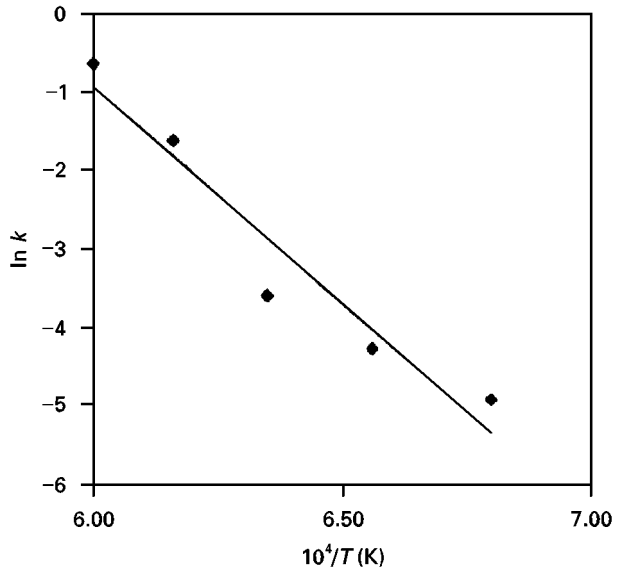


*Figure 9* Arrhenius plot of the parabolic oxidation rate constant as a function of absolute temperature for the base material.

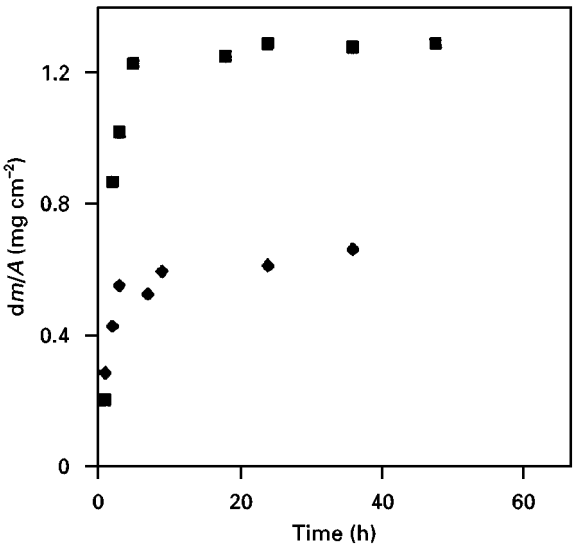


*Figure 11* Influence of TiC additions on the mass gain per unit area at an oxidation temperature of 1200 °C. (○), 0 wt% TiC; (■), 2 wt% TiC.

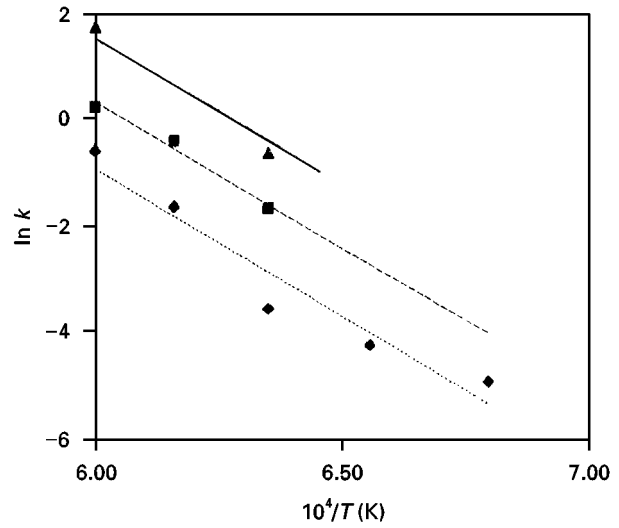


*Figure 10* Comparison between the activation energy for oxidation of $Si_3N_4$–$Y_2O_3$–$Al_2O_3$ with and without additions of TiC particles. (◆), 0 wt% TiC; (■), 2 wt% TiC; (▲), 10 wt% TiC.

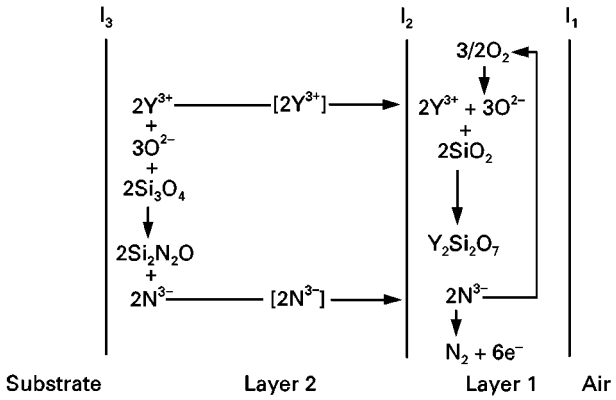


*Figure 12* Schematic representation of the development of the sublayers within the oxide scale.

The formation of a modified substrate layer (layer 2) due to the outward diffusion of $N^{3-}$ and $Y^{3+}$ results in a recession of interface $I_3$ with a velocity given by

$$\frac{dy}{dt} \approx \frac{D^*[P_N(I_3) - P_N(I_2)]}{dy}$$

$D^*$ being the effective diffusion coefficient for $Y^{3+}$ and $N^{3-}$. The thickness of the layer consisting of $Si_3N_4$ and $Si_2N_2O$ is governed by the rate of formation of such layer at interface $I_3$ and its consumption at interface $I_2$. The fact that the thickness of this layer in certain conditions (1200 °C) does not vary significantly with time indicates that $dx/dt \approx dy/dt$, which implies that the diffusion of $N^{3-}$ and $Y^{3+}$ represents a slow process with a rate comparable with that of oxygen diffusion. In contrast, in previously reported work [14] the oxidation behaviour of the reference material at a high temperature (1400 °C) was observed to proceed with the development of larger amounts of $Si_2N_2O$ in the subscale as the oxidation time increased. This is expected considering the fact that the temperature dependence for the diffusion of $Y^{3+}$–$N^{3-}$ is higher that that for oxygen diffusion (higher value for the activation energy). Consequently, the diffusion of $Y^{3+}$–$N^{3-}$ increases more rapidly with increasing temperature than does the oxygen diffusion. In these conditions the velocity with which the interface $I_3$ recedes exceeds that of interface $I_2$ and a modified layer of increasing thickness results.

Another observation in the present work which shows that the diffusion of $N^{3-}$ (and hence associated $Y^{3+}$) is a slow process is the development of $N_2$ bubbles near to interface $I_2$ which form as nitrogen from the reaction $N^{3-} + O_2 \rightarrow N_2 + O^{2-}$ is liberated. The oxygen ions formed in this way combine with $Y^{3+}$ and $SiO_2$, resulting in the kind of $Y_2Si_2O_7$ precipitate shown in Fig. 2.

In order to interpret the results observed for the materials with TiC additions, it is important to consider that TiC seems to be a readily oxidizable species on the experimental oxidation conditions. From this

point of view the larger mass gain observed in this material could be associated with the conversion of TiC into $TiO_2$ in addition to the formation of $SiO_2$ and $Si_2N_2O$ from the reaction between $Si_3N_4$ and oxygen. Since the activation energies are apparently the same for both materials, it could be thought that oxygen diffusion through the oxide scale is the controlling mechanism for the oxidation process. It is also possible that the larger mass gain observed for the TiC-containing materials arises because a more oxygen-permeable oxide scale is formed as a consequence of the incorporation of $Ti^{3+}$ as a modifier in its glassy structure. The fact that TiC exists in the lower part of the oxide scale may be attributed to the fact that, at the TiC–$SiO_2$ interface, important partial pressures of CO or $CO_2$ develop which may inhibit the further conversion of TiC into $TiO_2$. This shows that, as for the $Si_3N_4$ matrix, the oxidation of TiC may be considered as a process of mixed kinetics, determined by outward diffusion of CO–$CO_2$ and incoming $O_2$.

## 5. Conclusions

$Si_3N_4$-based materials containing additions of $Y_2O_3$ and $Al_2O_3$ show parabolic oxidation kinetics with an apparent activation energy of 460 kJ $mol^{-1}$, which suggests that the migration of metallic cations to the reaction interface is the controlling mechanism for the oxidation process.

The larger mass gains observed in the samples containing TiC additions seem to be associated with the formation of $TiO_2$ and with the lower viscosity of the glassy silicate due to the presence of $Ti^{3+}$ cations. The oxide scale formed in these compositions consists of an outer layer constituted by a glassy phase with dispersed crystals of $TiO_2$, $SiO_2$ and $Ti_2Y_2O_7$, and an inner sublayer in which $Ti_2Y_2O_7$, $SiO_2$, $Ti_2O_3$ and unreacted TiC were detected. The presence of unreacted TiC in the inner part of the oxidation scale suggests that the diffusion of CO or $CO_2$ may make a contribution to the oxidation rate of the TiC phase.

## References


1. C. CM. WU, K. R. MCKINNEY, R. W. RICE, W. C. MCDONOUGH, and S. W. FREIMAN, *J. Mater.* Sci. **16** (1981) 3099.
2. R. K. GOVILA, *ibid.* **22** (1987) 1193.
3. J. GURLAND, *Int. Mater. Rev.* **33 (**1988) 151.
4. S. T. BULJAN, and S. F. WAYNE, *Adv. Ceram. Mater.* **2** (1987) 813.
5. F. CASTRO, J. ECHEBERRIA, and M. FUENTES, *J. Mater. Sci. Lett.* **11** (1992) 101.
6. F. A. COSTA-OLIVERA, R. J. FORDHAM and J. H. W. DE WIT, Third European Ceramics Society Conference Vol. 3. (P. Duran and J. F. Fernandez (Eds.) Faenza Editrice Iberica, S.L., Madrid, Spain, 1993) p. 973.
7. C.-H. YEH and M.-H. HON, *Ceram. Int.* **21** (1995) 181.
8. F. PENI, J. CRAMPON, and R.DUCLOS, Third European Ceramic Society Conference, Vol. 3 (P. Duren and J. F. Fernandez (Eds.) Faenza Editrice Iberica, S.L. Madrid, Spain, 1993) p. 979.
9. S. T. BELLOSI, A. TAMPIERI, and Y. ZHEN LIU, *Mater. Sci. Engng* **A127** (1990) 115.
10. J. ECHEBERRÍA and F. CASTRO, in Proceedings of the First European Ceramic Society Conference, Vol. 3, Maastricht, 1989, (G. de With, R.A. Terpstra and Metselaar (eds.) Elsevier Applied Science, London, England, 1989) p. 527.
11. D. CUBICCIOTI, and K. H. LAU, *J. Amer. Ceram. Soc.* **61 (**1978) 512.
12. G. N. BABINI, A BELLOSI and P. VINCENZINI, *J. Mater. Sci.* **19** (1984) 1029.
13. D. R. CLARKE, in "Progress in nitrogen ceramics," edited by F. L. Riley (Martinus Nijhoff, Boston, MA, 1983), p. 421.
14. J. ECHEBERRÍA and F. CASTRO, in "Structural ceramics, processing, microstructure and properties", edited by J. J. Bentzen, J. B. Bilde-Sorensen, N. Christiansen, A. Horsewell and B. Ralph. Proceedings of the 11th Risø International Symposium on Metallurgy and Materials Science (Risø National Laboratory, Risø, Roskilde, Denmark 1990) p. 249.



*Received 9 June 1997*
*and accepted 5 February 1998*